PERGAMON

Solid-State Electronics 43 (1999) 625–631

SOLID-STATE ELECTRONICS

Effect of material parameters on the quantum efficiency of GaInAsSb detectors

Yuan Tian *, Tianming Zhou, Baolin Zhang, Hong Jiang, Yixin Jin

Changchun Institute of Physics, Chinese Academy of Sciences, Changchun 130021, People's Republic of China

Received 18 July 1998; received in revised form 21 August 1998; accepted 29 September 1998

Abstract

In this paper, a theoretical study of the effect of material parameters on the quantum efficiency of a homogeneous GaInAsSb infrared photovolatic detector is presented. The considerations are carried out for the near room temperature and 2.5 μm wavelength. The calculated results show that the quantum efficiency depends strongly on the carrier concentrations in the n- and p-regions. In addition, the absorption coefficient, the surface recombination velocities and the widths of the two regions also effect the quantum efficiency.

1. Introduction

Quaternary alloys GaInAsSb have caused much interest in the present technology of the choice for present and future photo-electronic devices [1], because they give a possible spectral range of 2–4 μm which is very important for environmental monitoring, optical fiber communication and infrared imaging systems [2, 3]. GaInAsSb alloys have been used to fabricate detectors [4, 5] and lasers [6].

Some figures of merit of infrared photovoltaic (IR PV) detectors, such as the detectivity (D^*) and the responsivity (R), are proportional to the quantum efficiency. For instance, D^* is given by [7]

$$D^* = R\sqrt{\frac{A_0\Delta f}{2qI\Delta f}} = \frac{\eta q\lambda}{hc}\sqrt{\frac{A_0}{2qI}} \tag{1}$$

where R is the responsivity of a detector, I is the current in a detector due to the generation and recombination processes, Δf is the noise bandwidth, A_0 is a detector's optical area and λ is the incident light wavelength. h, c and q are constants with their regular meaning. η is the detector's quantum efficiency. As shown in Eq. (1), the quantum efficiency is the important parameter in effecting the performance of detectors. Therefore it is necessary to discuss the effect of material parameters of detectors on the quantum efficiency.

The effect of the structure and material parameters of detectors on the quantum efficiency and the correlation between the quantum efficiency and other figures of merit of the PV detectors have led to the publication of some works in the literature. Rogalsky and Rutkowsky [8] solved the one-dimensional diffusion equation in PbSnTe to analyzed the quantum efficiency of PbSnTe one-dimensional diode. Rosenfeld and Bahir [9] showed a theoretical study of the effect of the direction of the incident light on the quantum efficiency of homogeneous HgCdTe photodiodes. Other interesting works [10, 11], based on the numerical analysis process, presented computer solutions for the two- and three-dimensional cases.

However, most of the published research does not deal with GaInAsSb IR PV detectors. Therefore, a theoretical study on the quantum efficiency of a homogeneous GaInAsSb IR PV detector is presented in this paper, in which the dependence of the quantum efficiency on the carrier concentrations, surface recombination velocities, material thicknesses and absorption coefficient is shown.

* Corresponding author. Tel.: +86-431-595-2215/232; e-mail: snmocvd@public.cc.jl.cn

0038-1101/99/$ - see front matter
PII: S0038-1101(98)00294-9

2. Detector structure and quantum efficiency

Our investigation focuses on the structure of n–p $Ga_xIn_{1-x}As_{1-y}Sb_y$ shown in Fig. 1, in which the lattice of the GaInAsSb quaternary allay is matched to GaSb [12]. The light is injected from the n-side or p-side. In the following, we will mainly discuss the case of the light injected from the n-side. When we assume that the uniform signal photon flux f, the number of incident photons cm^2/s unit bandwidth, is incident on the surface of the n-type GaInAsSb alloy, the generation rate of hole–electron pairs as a function of distance x from the surface is [13]

$$G = \alpha(\lambda)(1-r)\phi e^{-\alpha(\lambda)x} \tag{2}$$

where r is the reflection coefficient at the front surface. λ is the wavelength of the incident light and α denotes the absorption coefficient as a function of λ. In Eq. (2), the reflection coefficient at the back surface is neglected [14].

For simplicity, a one-dimensional model for the GaInAsSb detectors is taken. We assume low injection conditions and an abrupt junction. The influence of assuming a doping profile on detector performance has been solved by forward condition steady-state analysis [15]. Basic equations for d.c. analysis have the five well-known equations: two current density equations for electron J_e and hole J_h, two continuity equations for electrons and holes and Poisson's equation which are collectively referred to as the Van Roosbroeck model [16]:

$$J_e = qD_e\frac{dn}{dx} - q\mu_e n\frac{d\varphi}{dx} \tag{3A}$$

current density for electrons

$$J_h = -qD_h\frac{dp}{dx} - q\mu_h p\frac{d\varphi}{dx} \tag{3B}$$

current density for holes

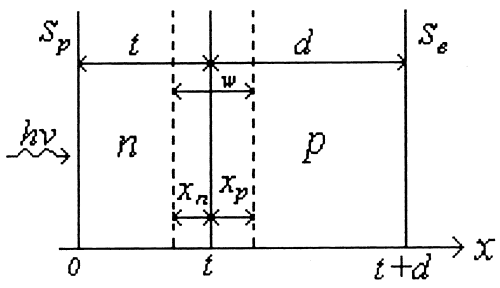

Fig. 1. The one-dimensional detector model.

$$\frac{1}{q}\frac{dJ_e}{dx} + (G-R) = 0 \tag{3C}$$

continuity equation for electrons

$$\frac{1}{q}\frac{dJ_h}{dx} - (G-R) = 0 \tag{3D}$$

continuity equation for holes

$$\frac{d^2\varphi}{dx^2} = -\frac{q}{\varepsilon_0\varepsilon_s}(N_d - N_a + p - n) \tag{3E}$$

Poisson′s equation

In Eqs. (3A)–(E), μ_e and μ_h are the electron and hole mobilities, D_e and D_h the electron and hole diffusion coefficients, n and p the electron and hole densities, φ the electrostatic potential, N_d the concentration of donors, N_a the concentration of acceptors and $\varepsilon_0\varepsilon_s$ the permittivity of the semiconductors, G and R denote the carrier generation and recombination rates, respectively.

To evaluate Eqs. (3A)–(E) the following bounding conditions are imposed to the carrier continuity equations [17]:

$$J_p = qS_n(p_n - p_{n0}) \quad (x=0) \tag{4A}$$

$$J_n = qS_p(n_p - n_{p0}) \quad (x = t+d) \tag{4B}$$

$$p_n - p_{n0} = \quad (x = x_n) \tag{4C}$$

$$n_p - n_{p0} = 0 \quad (x = t + x_p) \tag{4D}$$

Eqs. (4A)–(B) account for the front and back surface recombination velocities (S_e, S_p) characterizing the semiconductor surfaces and Eqs. (4C)–(D) state that the excess carrier densities are reduced to zero at the edge of the depletion region [13].

The detector is divided into a depletion region (x_n, $t + x_p$) and two quasi-neutral regions (0, x_n) and ($t + x_p$, $t + d$) respectively. Using these boundary conditions (Eqs. (4A)–(D)) in Eqs. (3A)–(E) and solving the simultaneous equations, the photocurrents per unit bandwidth for the three regions (J_n, J_p, J_{dr}), due to electrons collected at the junction edge, are given to be [13]:

$$J_n = \frac{q\phi(1-r)\alpha L_h}{\alpha^2 L_h^2 - 1}\left\{\frac{\alpha L_h + r_h - e^{-\alpha(t-x_n)}[r_h ch(t-x_n/L_h) + sh(t-x_n/L_h)]}{r_h sh(t-x_n/L_h) + ch(t-x_n/L_h)} - \alpha L_h e^{-\alpha(t-x_n)}\right\} \tag{5A}$$

$$J_p = \frac{q\phi(1-r)\alpha L_e}{\alpha^2 L_e^2 - 1} e^{-\alpha(t+x_p)}\left\{\frac{(r_e - \alpha L_e)e^{-\alpha(d-x_p)} - r_e ch(d-x_p/L_e) - sh(d-x_p/L_e)}{ch(d-x_p/L_e) + r_e sh(d-x_p/L_e)} + \alpha L_e\right\} \tag{5B}$$

$$J_{dr} = q\phi(1-r)[e^{-\alpha(t-x_n)} - e^{-\alpha(t+x_p)}] \tag{5C}$$

Therefore, the total photocurrent J_{ph} is given by

$$J_{ph} = J_n + J_p + J_{dr} \tag{6}$$

In general, the steady-state photocurrent density J_{ph} is [18]

$$J_{ph(f)} = qhf \tag{7}$$

Depending on Eqs. (5A)–(C), (6) and (7), the quantum efficiency of GaInAsSb detectors from the three regions (η_n, η_p, η_{dr}) and the total one (η) are shown as follows [8]:

$$\eta_n = \frac{(1-r)\alpha L_h}{\alpha^2 L_h^2 - 1}\left\{\frac{\alpha L_h + r_h - e^{-\alpha(t-x_n)}[r_h ch(t-x_n/L_h) + sh(t-x_n/L_h)]}{r_h sh(t-x_n/L_h) + ch(t-x_n/L_h)} - \alpha L_h e^{-\alpha(t-x_n)}\right\} \tag{8A}$$

$$\eta_p = \frac{(1-r)\alpha L_e}{\alpha^2 L_e^2 - 1} e^{-\alpha(t+x_p)}\left\{\frac{(r_e - \alpha L_e)e^{-\alpha(d-x_p)} - r_e ch(d-x_p/L_e) - sh(d-x_p/L_e)}{ch(d-x_p/L_e) + r_e sh(d-x_p/L_e)} + \alpha L_e\right\} \tag{8B}$$

$$\eta_{dr} = (1-r)[e^{-\alpha(t-x_n)} - e^{-\alpha(t+x_p)}] \tag{8C}$$

$$\eta = \eta_p + \eta_n + \eta_{dr} \tag{8D}$$

3. Discussions for the calculation results

The calculations have been performed on an n–p $Ga_{0.8}In_{0.2}As_{0.19}Sb_{0.81}$ PV detector operated at 300 K and 2.5 μm wavelength. The dependence of GaInAsSb alloy parameters such as energy bandgap and reflection coefficient that are necessary in calculations for the compositions x and y have been shown in Ref. [12]. For practical calculation, the hole mobility was fixed to be $\mu_h = 240$ cm^2/V s in the p-region and the electron one to be $\mu_e = 1000$ cm^2/V s in the n-region [19]. In addition, the incident light with 2.48 μm wavelength close to the intrinsic absorption edge in $Ga_{0.8}In_{0.2}As_{0.19}Sb_{0.81}$ is assumed to be injected from the n-region and then through the depletion region to reach the p-region. Depending on the injected light energy, the absorption coefficient is assumed to be $\alpha = 2.15 \times 10^5$ m^{-1} [20]. We also assume that the surface recombination velocities on both sides of the detector yield large electrical reflecting conditions for the holes and electrons, respectively.

All of the figures show the quantum efficiency obtained in the detector configuration as calculated from Eqs. (8A)–(D). Because the change of mobilities in the two regions has no influence on the quantum efficiency, we don't show their effect on the quantum efficiency. Except for the mobilities, the other parameters, such as the carrier concentrations, widths, surface recombination velocities in the two quasi-neutral regions and the absorption coefficient, all effect the quantum efficiency. Therefore, in calculation, we only give the relationship between the quantum efficiency and the two parameters, while the remaining parameters are kept constant.

Fig. 2 shows the quantum efficiency depending on the carrier concentration of the two quasi-neutral regions for $t = 0.5$ μm, $d = 5$ μm, $S_e = S_p = 0$. Fig. 2 distinctly shows that the total quantum efficiency (η) is mainly determined by the p-side quantum efficiency (η_p), while the n-side quantum efficiency (η_n) contributes little to η. In addition, the depletion region quantum efficiency (η_{dr}) has much effect on η only at a p-side carrier concentration less than 10^{14} cm^{-3} in Fig. 2(a). We also find in Fig. 2(a), that the maximal quantum efficiency obtained is almost 40% in the region 10^{13}–10^{18} cm^{-3} p-side carrier concentration meanwhile the n-side carrier concentration is assumed to be 10^{18}

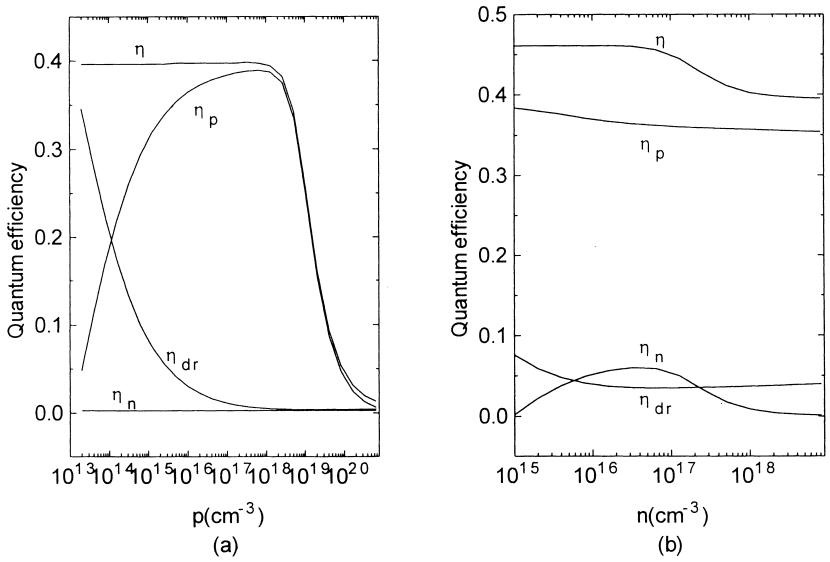

Fig. 2. The dependence of the quantum efficiency on the carrier concentration of (a) the p-region; (b) the n-region. In the calculations it is assumed: $t = 0.5$ μm, $d = 5$ μm, $S_e = S_p = 0$, $\alpha = 2.15 \times 10^5$ m^{-1}, $\mu_e = 1000$ cm^2/V s and $\mu_p = 240$ cm^2/V s.

cm^{-3}. In addition, as shown in Fig. 2(b), when the p-side carrier concentration is maintained at 6.4×10^{15} cm^{-3}, the maximal quantum efficiency will increase to 46% if the n-side carrier concentration is reduced to less than 10^{16} cm^{-3}. Fig. 2 indicates that the quantum efficiency will be improved with reduced n- and p-side carrier concentrations. This calculated result is different from the experiment results [19, 21], in which the n-side carrier concentration is assumed to be 10^{17}–10^{18} cm^{-3}.

Fig. 3 shows the quantum efficiency versus the p-side carrier concentration with the back surface recombination velocity (S_e), p-side width (d) or absorption coefficient (α) as a parameter, for $n = 10^{18}$ cm^{-3}, $t = 0.5$ μm, $S_p = 0$. From Fig. 3 it is indicated that increasing the back surface recombination from 0 to

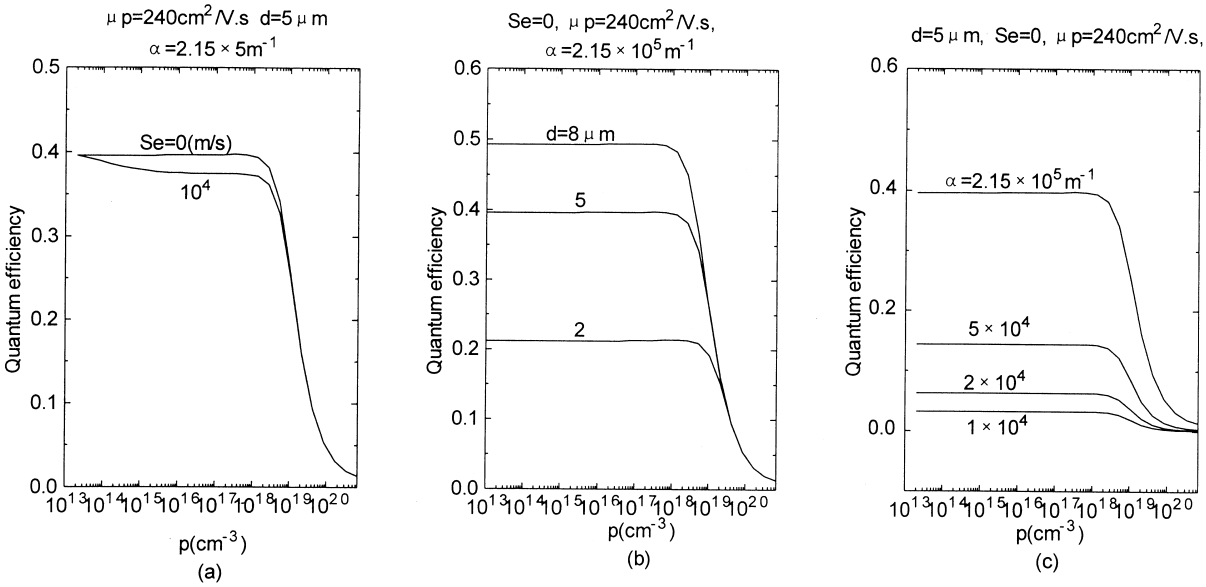

Fig. 3. The quantum efficiency versus the p-side carrier concentration (p) with (a) the back surface recombination velocity (S_e); (b) the p-side width (d); (c) the absorption coefficient (α) as a parameter. In the condition of $S_p = 0$, $t = 0.5$ μm, $n = 10^{18}$ cm^{-3}, $\mu_e = 1000$ cm^2/V s and $\mu_p = 240$ cm^2/V s.

10^4 m/s only reduces a little quantum efficiency, while the thicker width of the p-region and the larger absorption coefficient will obtain the higher quantum efficiency within $p < 10^{18}$ cm^{-3}. In order to find the widest thickness of the p-region for the maximal quantum efficiency, Fig. 4 shows the quantum efficiency as a function of the p-side width for $p = 6.4 \times 10^{15}$ cm^{-3} and other parameters, the same as in Fig. 3. Fig. 4 indicates that the quantum efficiency will reach a saturation value with an infinite thickness of the p-region and in corresponding to obtain the saturation detectivity. However it has been shown that the higher detectivity will be obtained with the thinner p-side width when the quantum efficiency is assumed to be 100% [12]. These different results require us renewably to analyze the effect of the p-side width on the detectivity when the quantum efficiency is considered in the detectivity, which will be discussed in another paper.

The relationship between the quantum efficiency and the n-side carrier concentration with the front surface recombination velocity (S_p), n-side width (t) and absorption coefficient (α) is shown in Fig. 5 for $p = 6.4 \times 10^{15}$ cm^{-3}, $d = 5$ μm, $S_e = 0$. The quantum efficiency in Fig. 5(a) and (c) is similar to the one in Fig. 3(a) and (c), respectively, where the maximal quantum efficiency obtained requires reduction of not only the front surface recombination velocity (S_p) but also of the back one (S_e), on the contrary to increase the absorption coefficient. In Ref. [20], the absorption coefficient is dependent on the incident light energy (hv):

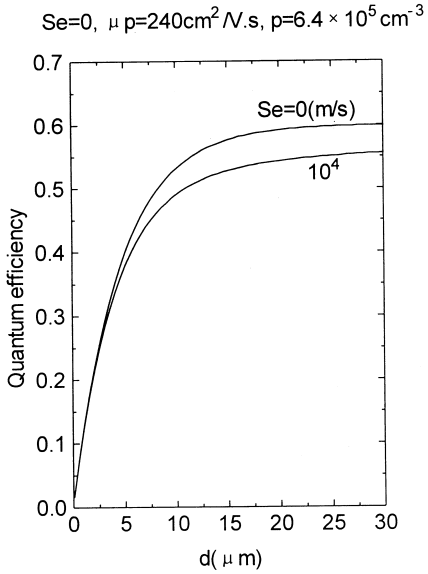

Fig. 4. The quantum efficiency versus the p-side width (d) with the back surface recombination velocity (S_e) as a parameter. Other parameters are the same as in Fig. 3.

$$\alpha \propto \sqrt{(1/hv) - (\mathrm{Eg}/hv^2)}$$

where Eg is the GaInAsSb bandgap energy. Inserting this equation in Eqs. (8A)–(D), the calculated result shows that the incident light energy should be decreased to the band edge absorption in order to get the maximal η.

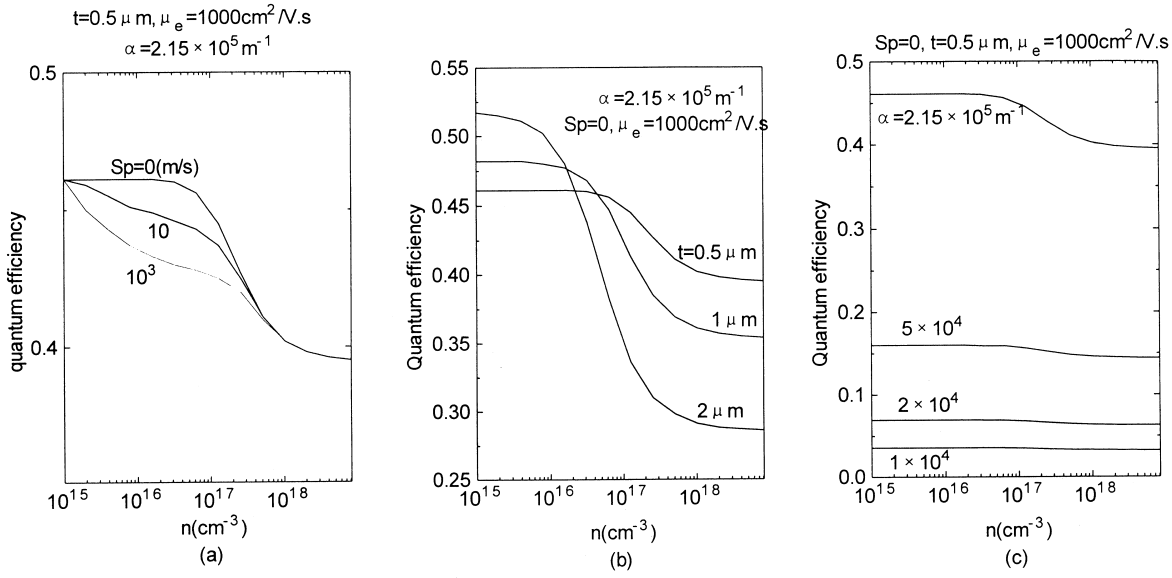

Fig. 5. The quantum efficiency versus the n-side carrier concentration (n) with (a) the front surface recombination velocity (S_p); (b) the n-side width (t); (c) the absorption coefficient (α) as a parameter. In the condition of $S_e = 0$, $d = 5$ μm, $p = 6.4 \times 10^{15}$ cm^{-3}, $\mu_e = 1000$ cm^2/V s and $\mu_p = 240$ cm^2/V s.

A confusing phenomena appears in Fig. 5(b), for which it is difficult to select the optimum n-side width and carrier concentration for the maximal quantum efficiency. However, when the variable and parameter in Fig. 5(b) reciprocate each other, the clear relationship between the quantum efficiency and the n-side width with the carrier concentration as a parameter is shown in Fig. 6. Due to the complex relationship between η and t in Eqs. (8A)–(D), η appears as a peak with varying n-side carrier concentration and the peak increases and tends to the great width of the n-region with decreasing n-side carrier concentration. Decreasing the n-side carrier concentration improves the quantum efficiency, which coincides with that in Fig. 2(b). Meanwhile, the n-side width needs to be adjusted to obtain high quantum efficiency.

4. Conclusion

In this paper, a theoretical study of the effect of material parameters of a $Ga_{0.8}In_{0.2}As_{0.19}Sb_{0.81}$ IR PV detector on the quantum efficiency at 300 K has been carried out. The quantum efficiency dependent on the absorption coefficient, the carrier concentrations, widths and surface recombination velocities in the p- and n-regions is calculated. The calculated results show that the higher quantum efficiency needs the incident light energy near to the GaInAsSb band edge energy and is obtained by reducing the carrier concentrations in the n- and p-regions. Moreover, a peak of η appears by varying the n-side width in the range of the low n-side carrier concentration. In addition, the higher quantum efficiency is obtained by reducing the surface recombination velocities, either the front one or the back one. It is also shown that the quantum efficiency reaches a saturation value with an infinite thickness of the p-region.

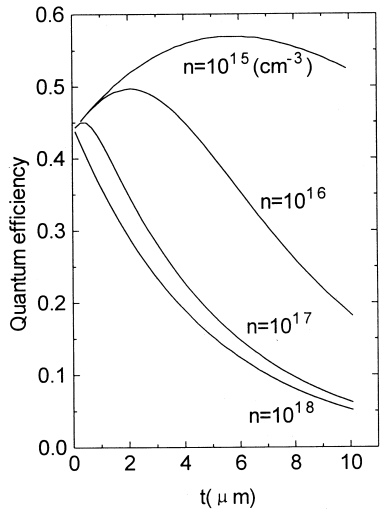

Fig. 6. The quantum efficiency versus the n-side width (t) with the n-side carrier concentration (n) as a parameter. Other parameters are the same as in Fig. 5.

The results in this paper are obtained under the condition of neglecting degeneracy in a $Ga_{0.8}In_{0.2}As_{0.19}Sb_{0.81}$ alloy because little degenerated state exists in the material at a carrier concentration larger than 10^{20} cm^{-3}. Therefore, in this paper's calculation and analysis, we neglect the effect of degeneracy and thus we can get clear and concise results that are very useful for us for further research work in the future.

Acknowledgements

This paper is supported by the National Advanced Materials Committee of China (NAMCC).

References

[1] Benoit J, Boulou M, Soulage G, Joullie A, Mani H. J Opt Commum 1988;9(2):55–8.
[2] Aardvark A, Allogho GG, Bougnot G, David JPR, Giani A, Haywood SK, Hill G, Klipstein PC, Mansoor F, Mason NJ, Nicholas RJ, Pascal-Delannoy F, Pate M, Ponnampalam L, Walker PJ. Semicond Sci Technol 1993;8(1S):S380.
[3] Srivastava AK, Dewinter JC, Caneau C, Pollack MA, Zyskind JL. Appl Phys Lett 1986;48(14):903.
[4] Zhang B, Zhou T, Jiang H, Ning Y, Jin Y. Electron Lett 1995;31:830.
[5] Zhang B, Jin Y, Zhou T, Jiang H, Ning Y, Li S. Mar Res Soc Symp Proc 1996;415:31.
[6] Choi HK, Eglash SJ. Appl Phys Lett 1991;59:1165.
[7] Willardson RK. Semicoductors and semimetals, vol. 18. . New York, 1981. p. 236.
[8] Rogalski A, Rutkowski J. Infrared Phys 1982;22:199.
[9] Rosenfeld D, Bahir G. J Appl Phys 1992;72:3034.
[10] Levy D, Schacham SE, Kidrom I. IEEE Trans Electron Devices 1987;34:2059.
[11] Levy D, Schacham SE, Kidrom I. IEDM Tech Dig 1986;18:373.
[12] Tian Y, Zhou TM, Zhang BL, Jin YX, Ning YQ, Jiang H, Yuan G. Opt Eng 1998;37(6):1754.
[13] Willardson RK, Beer AC. Semiconductors and semimetals, vol. 11. Academic Press, 1975. p. 16.
[14] Djuric Z, Jaksic Z. Electron Lett 1988;24:1100.
[15] Kurata M. Numerical analysis of semiconductor device. Toronto: Lexington, 1982.
[16] Van Roosbroeck W. Bell Syst Tech J 1950;29:560.

[17] van der Wiele F. In: Jespers PG, van der Wiele J, White MH. Solid state imaging. Noordhoff: Leydon, 1976. p. 47.
[18] Willardson RK, Beer AC. Semiconductors and semimetals, vol. 18. Academic Press, 1981. p. 228.
[19] Li AZ, Zhong JQ, Zheng YL, Wang JX, Ru GP, Bi WG, Qi M. J Cryst Growth 1995;150:1375.
[20] Moss TS, Burrell GJ, Ellis B. Semiconductor opto-electronics. Chapel River Press, 1973. p. 48.
[21] Mebarki M, Ait-Kaci H, Lazzari JL, Segura-Fouillant C, Joullie A, Llinares C, Salesse I. Solid-State Electron 1996;39(1):39.